Biomaterials 77 (2016) 255–266

Contents lists available at ScienceDirect

Biomaterials

journal homepage: www.elsevier.com/locate/biomaterials

Effect of prevascularization on *in vivo* vascularization of poly(propylene fumarate)/fibrin scaffolds

Ruchi Mishra [a], Brianna M. Roux [b, c], Megan Posukonis [a, 1], Emily Bodamer [a, 1], Eric M. Brey [b, c], John P. Fisher [d], David Dean [a, *]

[a] Department of Plastic Surgery, The Ohio State University, Columbus, OH, USA
[b] Department of Biomedical Engineering, Illinois Institute of Technology, Chicago, IL, USA
[c] Research Service, Edward Hines Jr. V.A. Hospital, Hines, IL, USA
[d] Fischell Department of Bioengineering, University of Maryland, College Park, MD, USA

ARTICLE INFO

Article history:
Received 5 August 2015
Received in revised form
11 October 2015
Accepted 12 October 2015
Available online 22 October 2015

Keywords:
Mesenchymal stem cells (MSCs)
Human umbilical vein endothelial cells (HUVECs)
Poly(propylene fumarate) (PPF)
Fibrinogen
Thrombin

ABSTRACT

The importance of vascularization in the field of bone tissue engineering has been established by previous studies. The present work proposes a novel poly(propylene fumarate) (PPF)/fibrin composite scaffold for the development of vascularized neobone tissue. The effect of prevascularization (i.e., *in vitro* pre-culture prior to implantation) with human mesenchymal stem cells (hMSCs) and human umbilical vein endothelial cells (HUVECs) on *in vivo* vascularization of scaffolds was determined. Five conditions were studied: no pre-culture (NP), 1 week pre-culture (1P), 2 week pre-culture (2P), 3 week pre-culture (3P), and scaffolds without cells (control, C). Scaffolds were implanted subcutaneously in a severe combined immunodeficiency (SCID) mouse model for 9 days. During *in vitro* studies, CD31 staining showed a significant increase in vascular network area over 3 weeks of culture. Vascular density was significantly higher *in vivo* when comparing the NP and 3P groups. Immunohistochemical staining of human CD-31 expression indicated spreading of vascular networks with increasing pre-culture time. These vascular networks were perfused with mouse blood indicated by perfused lectin staining in human CD-31 positive vessels. Our results demonstrate that *in vitro* prevascularization supports *in vivo* vascularization in PPF/fibrin scaffolds.

1. Introduction

The formation of strong bone requires a remodeling process that results in a highly organized array of osteocytes [1]. The mineralized extracellular matrix (collagen I and hydroxyapatite) surrounding these osteocytes includes a dense and profuse vascular supply [2]. The vascular supply of bone is required for providing oxygen and nutrients and acts as a conduit for new osteoprogenitor cells needed to maintain the newly formed bone [3]. Engineering functional bone requires the generation of an extensive microvascular network within the resultant tissue.

Bone tissue engineering aims to regenerate bone tissue through the development and application of bone tissue engineered grafts. These grafts are expected to be functionally active at the defect site and support the healing process, and, thereafter resorb at a rate compatible with the remodeling of the newly formed bone. Tissue engineered bone grafts typically consist of resorbable scaffolds prepared from polymeric, ceramic, and composite biomaterials along with cells and growth factors [4]. As yet, other than the Infuse (Medtronic, Minneapolis, MN) product, none has proved sufficient for healing critical-size or larger bone defects (i.e., 2–3 cm or greater) [5]. It is often because bone grafts of such sizes do not receive adequate supply of oxygen and nutrients at the inner regions of the graft, a necrotic core forms defeating the researcher's regenerative bone strategy. Therefore, it is critically important to establish a vascular supply throughout a graft, especially in large bone grafts, for successful bone regeneration to take place [6,7].

With an increase in the understanding of bone healing, the number of studies acknowledging the importance of vascularization in bone healing has increased [8,9]. Three frequently explored *in vitro* strategies for establishing a vascular supply in bone tissue

* Corresponding author. Department of Plastic Surgery, The Ohio State University, 460 West 12th Ave., 10th Floor, Rm. 1004, Columbus, OH 43210, USA.
E-mail address: David.Dean@osumc.edu (D. Dean).
[1] Authors contributed equally to this work.

http://dx.doi.org/10.1016/j.biomaterials.2015.10.026
0142-9612/

engineered scaffolds are: 1) stimulation of vascularization from surrounding tissue via incorporation of growth factors or other proangiogenic stimuli [10], 2) bioreactor culture, and/or, 3) co-culture of endothelial cells along with mesenchymal stem cells or osteoblasts [11]. Bioreactors provide an artificial proxy for vascularization via continuous in-flux of nutrients and oxygen and out-flux of waste materials through the bioreactor system [12–17]. On the other hand, co-culture with endothelial cells (e.g., model cell types such as HUVECs or endothelial progenitor cells [EPCs]), establishes natural vascularization within the scaffold via the formation of blood vessels [18,19].

Another important method for establishing vascularization of a three dimensional scaffold is *in vivo* vascularization. This can be carried out in two possible ways: 1) Extrinsic vascularization via implantation and incubation of the scaffold beneath a highly vascularized region of the body such as subcutaneous tissue for a certain interval of time before implantation at the defect area, and, 2) Intrinsic vascularization though implantation of a vascular network into the scaffold which is further anastomized with the surrounding host vasculature through surgical intervention [48].

Co-culture of endothelial cells along with osteoblasts has been found to be favorable for bone formation and vascularization [20–23]. hMSCs and endothelial cell co-culture has been studied for the interplay and interaction of the two cell types for promoting osteogenic differentiation and vascularization *in vitro* [24]. These cells can be incorporated by co-seeding on the biomaterial scaffolds or culturing them in the form of three-dimensional spheroids [25]. Spheroid co-culture is advantageous in comparison with direct seeding of bone and blood vessel progenitor cells because it provides an environment similar to that of the body, where tissues are made up of more than one kind of cell arranged in 3 dimensional configurations [26]. Synergistic/co-stimulatory effects of hMSC/HUVEC spheroid co-culture have been studied. HUVECs not only form vascular networks but also promote osteogenesis and proliferation of hMSCs [27–30]. The hMSCs lead to bone formation while acting as trophic mediators for endothelial cells by secreting proangiogenic factors and acting as a scaffold for the formation and stabilization of vascular units [31,32].

Despite the importance of vascularization in bone tissue engineering, there is still a need to improve upon current methods for the prevascularization of bone tissue engineering scaffolds. Combining these prevascularization strategies with resorbable scaffolding biomaterials could ensure the appropriate size and shape of the forming bone [31]. Poly(propylene fumarate) polymer is a photocrosslinkable, biocompatible and resorbable biomaterial which can be 3-D printed into almost any desirable shape and size and can be rendered with high mechanical strength [33,34]. PPF has also been extensively studied for bone tissue engineering applications [33,35–38], though, the vascularization of these scaffolds is less studied [39–43]. Fibrin, which is formed naturally in the body during wound healing [44], is widely used to enhance vascularization due to its pro-angiogenic properties. However, its mechanical properties are less suitable for bone tissue engineering applications.

A recent study from our group evaluated the vascularization potential of PPF scaffolds through modeling and experimental studies based on 3D printed structure [34]. Incorporation of fibrin polymers into PPF as a composite system that combines the favorable properties of both the polymers for vascularization of bone tissue engineered scaffolds as well as to maintain the space of the defect have not been studied to our knowledge. We speculate that a composite scaffold of PPF and fibrin could provide a mechanically stable biomaterial system that facilitates vascularization (Fig. 1). Therefore, we developed a novel composite scaffold system of fibrin and a 3-D printed poly(propylene fumarate) shell in which we can study the effect of hMSC/HUVEC spheroid pre-culture on the vascularization of these scaffolds for bone tissue engineering applications. In the present study, our overall aim is to study the effect of *in vitro* spheroid pre-culture/prevascularization on *in vivo* vascularization response inside this clinically scalable scaffold system.

2. Methods

2.1. Experimental design

Each scaffold sleeve consisted of a fibrin hydrogel containing a single HUVEC/hMSC spheroid. Experiments were conducted in an organized manner. For the *in vitro* experiments, scaffolds were cultured for 1, 2, or 3 weeks ($n = 3$ per time point) prior to formalin fixing. Samples were stained for human CD-31 and α-SMA and imaged using confocal microscopy. The *in vivo* experiments involved five experimental groups with five mice each receiving four scaffolds subcutaneously. Therefore, each group consisted of twenty scaffolds. On the basis of the time of *in vitro* pre-culture of the fibrin-embedded spheroid before implantation, the experimental groups were as follows: 1) No pre-culture (NP) group, 2) 1 week pre-culture (1P) group, 3) 2 week pre-culture (2P) group, 4) 3 week pre-culture (3P) group, and 5) control (C) group (i.e., a solid-cured, resorbable polymeric sleeve containing fibrin without a spheroid). All groups were implanted for 9 days immediately following the group's respective pre-culture time. Mice from each group were sacrificed at the corresponding time point and a formaldehyde perfusion fixation procedure was undertaken. Out of the twenty scaffolds obtained per group, 8 were used for lectin imaging while 12 scaffolds were used for other histological analysis. Out of the 8 lectin imaged scaffolds, 3 were used for overall *in vivo* fluorescence imaging before preparing them for microscopic analysis.

2.2. Synthesis and sterilization of scaffold sleeves

Poly(propylene fumarate) (PPF) (Molecular weight = 1269 Da, PDI = 1.5) cylindrical sleeves were printed using an EnvisionTEC (Dearborn, MI) Perfactory 3 Standard 3D Printer. The resin chemistry involved is 1:1 PPF:DEF, 0.7% w/w Irgacure 819/BAPO, 0.4% w/w Oxybenzone/2-Hydroxy-4-methoxybenzophenone and 0.3% w/w Irgacure 784. Hollow, cylindrical scaffolds with dimensions of 6 mm height, 3 mm outer diameter, 0.25 mm wall thickness, and 0.35 mm pore size were built (Fig. 1). The scaffolds were washed in a sterile environment to remove any uncured resin using the following sequence: 15 min PBS, 30 min 70% acetone, three times each of 15 min PBS, 20 min 70% acetone, three times each of 10 min 70% acetone, two times each of 15 min PBS. The scaffolds were placed in fresh PBS and incubated at 37 °C in a petri dish for 72 h following by soaking in FBS for two nights. The washed scaffolds were placed upright on a petri dish and incubated at 37 °C until dry.

2.3. Cell culture and spheroid preparation

HUVECs were purchased at passage P1, cultured to confluency in EGM-2 media and seeded into spheroids at passage P4. hMSCs were cultured to confluency in T-175 flasks using hMSC differentiation basal medium and seeded at passage P5 into spheroids. Both HUVECs and hMSCs were obtained under an exemption from the IRB since they were purchased and were received de-identified from the vendor. Spheroids of 2500 HUVECs and 2500 hMSCs were created by suspending cells in 150 μL EGM-2 containing 0.25% w/v methylcellulose. Spheroids were incubated overnight in

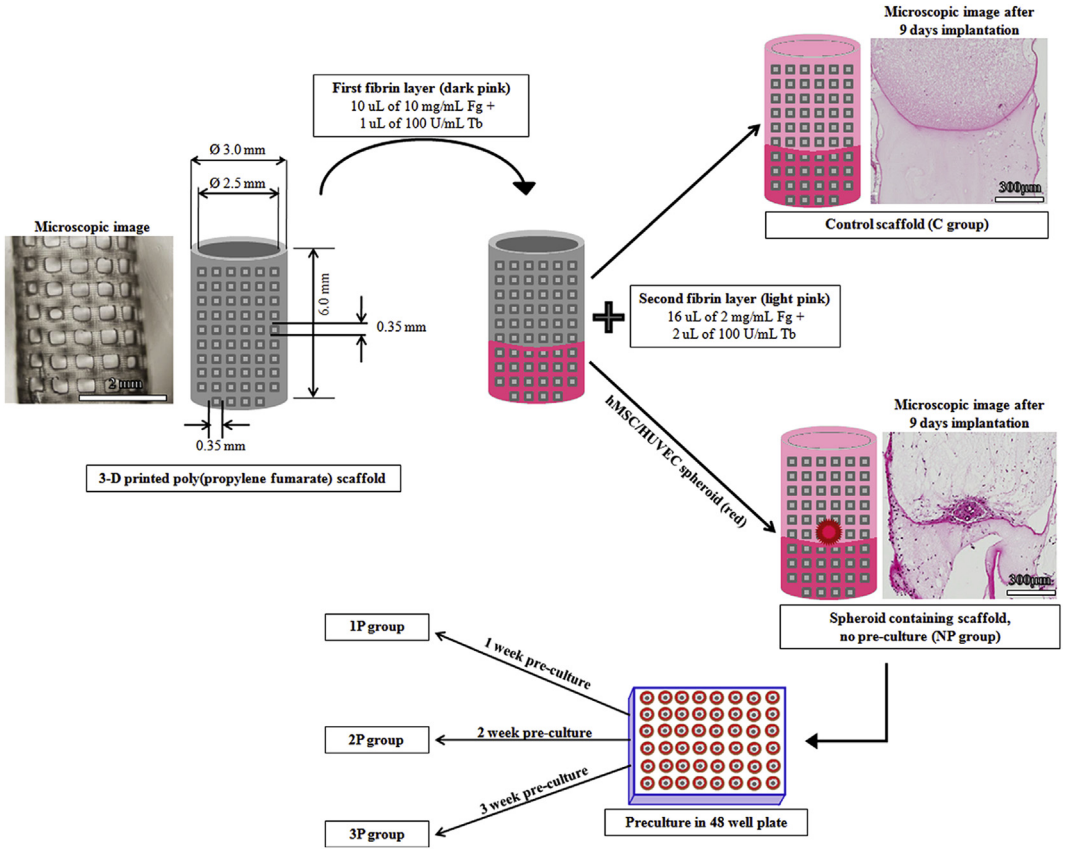

Fig. 1. Schematic representation of control and spheroid containing scaffold formation via fibrin loading inside porous 3-D printed poly(propylene fumarate) (PPF) scaffolds. An illustrative image of the 3-D printed PPF scaffold is shown along with that of a control and a spheroid containing scaffold after 9 days of implantation in a SCID mouse. Representation of poly(propylene fumarate)/fibrin scaffold dimensions is made by using SOLIDWORKS® (Dassault Systeme, Waltham, MA, USA) software. The PPF sleeve has a light grey color while the fibrin hydrogel has a dark grey color. Fibrin hydrogel is present inside the hollow sleeve and fills the pores of the sleeve forming a composite structure. The respective groups formed after preculturing the spheroid-containing scaffolds at different time points in a 48 well plate, i.e., 1P, 2P and 3P, are also indicated.

non-TC treated U-bottom 96 well plates in a cell culture incubator at 37 °C and 5% CO_2 before isolation for seeding into the fibrin scaffolds.

2.4. Fibrin and spheroid loading procedure

Fresh 1X phosphate buffered saline (PBS) was created from 10X PBS, sodium bicarbonate, and deionized water, and used for all stock and working solutions. Fresh working solutions of 2 mg/mL and 10 mg/mL human fibrinogen (Fg) were created from 100 mg/mL stock. Fresh working solution of 100 U/mL bovine thrombin (Tb) was created from a 1000 U/mL stock. Bovine and human thrombin have similar reaction kinetics and binding affinity for human fibrinogen [45]. All stock and working Fg and Tb solutions were stored on ice until loading.

Intact cell spheroids were extracted from the well plate to a petri dish containing ~5 mL PBS using a cut 200 μL pipette tip. The first layer of fibrin gel was created by combining 10 μL of 10 mg/mL Fg and 1 μL of 100 U/mL Tb and inserted into the scaffold using a gel-loading pipette tip. The scaffold and gel were incubated at 37 °C for 10 min to allow the fibrin gel to form. A single spheroid is then extracted from the PBS using a 200 μL pipette tip and inserted atop the first gel layer within the scaffold along with the second layer consisting of 16 μL of 2 mg/mL Fg and 2 μL of 100 U/mL Tb. The scaffold was again allowed to incubate for 10 min at 37 °C in a cell culture incubator to allow the gel to form. The bi-layer method, depicted as a schematic in Fig. 1, documents the higher fibrinogen concentration in the bottom layer. This stiffening prevents spheroid loss and ensures the spheroid is within the bulk of the scaffold. The scaffolds were transferred to a 48 well plate containing 500 μl media/scaffold/well for 1, 2, or 3 weeks of culture. Scaffolds were regularly monitored via brightfield microscopy on an Axiovert 200 inverted microscope (5x objective, 1.25 μm/pixel) and imaged every 2–3 days using an Axiovision AC 4.5 (Carl Zeiss, Germany). For imaging, the scaffolds were placed vertically in the culture well and mosaic images were taken such that the entire axial cross-section of the scaffold was visible. Media was changed every second day until the end of the pre-culture period, at which time samples were formalin-fixed (for the *in vitro* experiment) or implanted (for the *in vivo* experiment).

2.5. Immunofluorescence staining for vascular network formation in vitro

For the *in vitro* experiments, immunofluorescence staining was performed for CD31, an endothelial cell marker, and α-smooth muscle actin (αSMA), expressed by hMSCs [46]. Following fixation in 10% buffered formalin (Fisher Scientific, Pittsburgh, PA), samples were washed with PBS, permeabilized with 0.5% Triton-X in PBS (PBST), and blocked with 6% normal goat serum (MP Biomedicals, Solon, OH) for 1 h. Samples were incubated with 1:200 mouse anti-human CD31 (clone JC70A, Dako, Carpenteria, CA) and 1:600 rabbit anti-αSMA (polyclonal, Abcam, Cambridge, MA) primary antibodies with 2% normal goat serum in 0.5% PBST overnight at 4 °C. The

following day, samples were washed in fresh 0.5% PBST, and incubated with 1:200 TRITC-conjugated goat anti-mouse IgG and 1:200 FITC-conjugated donkey anti-rabbit IgG secondary antibodies (Jackson Immuno, West Grove, PA) in 0.5% PBST for 4 h at room temperature. All samples ($n = 3$ per timepoint) were imaged with a Zeiss LSM 5 PASCAL confocal microscope (5x objective, 3.57 μm/pixel), and placed vertically such that the entire axial cross-section of the scaffold was visible. Two-dimensional projections of the three-dimensional z-stack images were created using Pascal software (Carl Zeiss, Germany). The area of the CD31-positive cellular network was manually outlined and measured for all samples using Axiovision AC 4.5 (Carl Zeiss, Germany).

2.6. Animal model

All procedures were performed at the Biomedical Research Tower at The Ohio State University under an Institutional Animal Care and Use Committee approved protocol. The spheroid- and fibrin-loaded scaffolds were subcutaneously implanted into 8 week old, male, SCID C.B17 mice.

2.7. Surgical procedure for scaffold implantation

All mice were anesthetized through a nose cone under isoflurane, shaven, and were sterilized with ethanol followed by a betadine scrub. Subcutaneous incisions were made on the proximal and distal aspect of each limb, and four tunnels (one on each limb) were formed using blunt dissection [47]. The scaffolds were implanted along the tunnel axis and wounds were closed with wound clips. During the implant procedure marcaine was administered subcutaneously at each implantation site at a dose of 2 mg/kg divided among the four implant sites as a local anesthetic. Buprenorphine was used as the primary method of pain management and was subcutaneously injected immediately after the surgery and 24 h following at a dose of 0.1 mg/kg. Carprofen was administered at a dosage of 5 mg/kg at the same time points as a subcutaneous injection for use as both an analgesic as well as an anti-inflammatory drug. Upon completion of experiment, the primary method used for euthanasia was exsanguination followed by secondary euthanasia via cervical dislocation.

2.8. Scaffold extraction and tail vein injection

Nine days after implantation the mice were perfused with 4% paraformaldehyde. A gavage needle hooked to a perfusion pump was inserted in the left ventricle and the right auricle was cut to drain the animal's circulatory system of blood. The pump first flushed the circulatory system with saline then 4% paraformaldehyde was perfused by switching the input of the pump. The extracted scaffolds were stored in 4% paraformaldehyde for 24 h before performing the histological procedures. Whereas, for lectin staining two mice from each experimental group were randomly selected to receive isolectin Alexa Fluor 647 through a tail vein injection. The isolectin was injected at a concentration of 50 μg/100 μl prepared in 0.1–1.0 mM $CaCl_2$ (Fisher Scientific, Pittsburgh, PA, USA) containing phosphate buffered saline (PBS). A volume of 200 μl of this solution was injected using a sterile 28 gauge insulin syringe and lectin was allowed to circulate at least 15 min in the animal before anesthetizing for euthanasia/fixation. Thereafter, formalin fixation was performed and the scaffolds harvested from these isolectin-injected mice were placed in Optimal Cutting Temperature (OCT) and stored at −80 °C as frozen specimens. The scaffolds explanted from the remaining three mice were stored in 10% Neutral Buffered Formalin at room temperature for paraffin embedding and histological analysis.

2.9. Histological analysis for tissue invasion

A total of 5 slides were stained per group per animal and the imaging was performed at a standardized plane. The method of sectioning was as follows: from the top of the paraffin block, 100 micron deeper level was reached to get the section of the entire scaffold along with fibrin. After 100 micron depth, 5 sections were taken at each deeper level (1–5) of 70 micron depth difference so that we could cover a significant part of the scaffold without losing it while sectioning.

2.9.1. H&E staining

Sections of 4 μm thicknesses were first de-paraffinized in xylene followed by hydration with distilled water. Thereafter, these sections were stained with hematoxylin (Leica 560 MX) (Leica Biosystems Inc., IL, USA) for 8 min followed by steps including treatment with 1% acid alcohol, 1% ammonium hydroxide and rinsing in tap water. Finally the sections were stained in Eosin Y (Leica 515) (Leica Biosystems Inc.) after rinsing in tap water. Once both hematoxylin and eosin staining were complete, the sections were dehydrated in 95% ethanol in 2 changes of 12 dips each followed by 2 changes in 100% ethanol of 12 dips each and lastly cleared in xylene (Fisher Scientific). The stained and cleared sections were then cover slipped and viewed under the microscope.

2.9.2. Masson's trichrome staining

De-paraffinized sections of 4 μm thickness were first hydrated in distilled water and then stained in Weigert's hematoxylin (Poly Scientific R&D Corp., NY, USA) for 10 min followed by washing in tap water for another 10 min. These sections were further treated sequentially with Biebrich Scarlet Acid Fuchsin (Poly Scientific R&D Corp.), phosphomolybdic/phosphotungstic acid (Poly Scientific R&D Corp.), Aniline Blue (Poly Scientific R&D Corp.), and, 1% Glacial Acetic Acid A rinsing step with tap water was performed after each treatment. Once they were stained, the sections were dehydrated, cleared and mounted in the same procedure as mentioned in the H&E protocol (see previous section).

2.10. Immunohistochemistry staining of human CD-31

The sections were de-paraffinized and hydrated as previously mentioned in the H&E and Masson's trichrome staining protocols. Thereafter, these were pretreated in Target Retrieval Solution (Dako North America, Inc., CA, USA) and then washed in water for 5 min and rinsed in distilled water. Next, the sections were treated with 3% Hydrogen Peroxide in methanol for 10 min and rinsed in distilled water. Further, antibody staining and protein blocking was performed by incubating with primary anti-human CD-31 antibody diluted to 1:250 in Dako antibody diluent (Dako North America, Inc.) with background reducing agents for 30 min followed by incubation with biotinylated goat anti-rabbit diluted 1:200 in protein block (Dako North America, Inc.) for 30 min. Later, sections were incubated in Vector RTU ABC Elite complex (Vector Laboratories, Inc., U.S. Headquarters, Burlingame, CA, USA) for 30 min, rinsed in wash buffer followed by water. At this point, the sections were incubated in 3,3′-Diaminobenzidine (DAB) (Dako North America, Inc.) for 5 min and counterstained in hematoxylin for 30 s. Finally, the stained sections were rinsed in running tap water and treated with 1% Ammonium Hydroxide solution. The sections were then dehydrated, cleared and mounted in the same manner as discussed in above histological staining procedures.

2.11. Quantitative lectin imaging of explanted scaffolds using an in vivo imaging system (IVIS)

The imaging was performed in Optical imaging system IVIS Lumina II. The whole scaffolds of control and 3P groups explanted (n = 3) from the mice after isolectin injection were imaged for measuring epi-fluorescence under emission filter = Cy5.5 and excitation filter = 640 nm. Here, epi-fluorescence is measured in terms of total fluorescence radiant efficiency having the unit as photons s^{-1} cm^{-2} $steradian^{-1}$ per μW cm^{-2}.

2.12. Quantitative estimation of vessel density

Vessel density was calculated manually by dividing the number of vessels obtained in an image by the tissue area for that particular image. These vessels were identified via CD-31 staining. The plane of all the images was standardized at a depth of ~560 microns. In order to avoid biases, the quantification analysis was duplicated by another lab member. The vascular area per section was identified via overall image analysis of the whole longitudinal section. Further, average vessel density was calculated using 5 images/group types from the images of the 12 scaffolds obtained from 3 mice except group 2P for which the number of images was 3 due to loss of 2 samples to a technical error in sample processing. All images used for the analysis were kept at the same scale (scale bar = 300 μm) to maintain consistency across the calculations.

2.13. Cryosectioning and DAPI (4′,6-diamidino-2-phenylindole) staining for microscopic lectin imaging

A total of 8 scaffold sections obtained from 2 animals were used for this analysis. The OCT embedded scaffolds were sectioned using a cryo-microtome to obtain 20 μm thick sections at a standardized plane. These sections were obtained on glass slides which were further incubated in a coplin jar containing DAPI (Life Technologies, Carlsbad, CA) dye at a concentration of 2 drops/ml in PBS buffer for 5–10 min. After DAPI staining, the sections were mounted with a coverslip using Thermo Scientific Shandon™ Immu-Mount™ (Fisher Scientific) as a mounting media. These slides were allowed to air dry for at least 5–6 h before imaging in dark.

2.14. Microscopic lectin and human CD-31 florescence imaging under confocal microscope

Confocal microscopy imaging was performed on an Olympus (Center Valley, PA, U.S.A) Fluoview 1000 confocal microscope and images were analyzed via an Olympus FV10ASW V3.0 software. The imaging for vessel formation (lectin) and cell nuclei (DAPI) was performed at Ex/Em (excitation/emission) = 633 nm/670 nm and Ex/Em = 360 nm/460 nm, respectively. The images were superimposed in order to view the vessels and nuclei in their normal spatial relationship. Further, fibrin was identified along with vessels and nuclei using a differential interference contrast (DIC) detector. For human CD-31 fluorescence staining, the same primary antibody was used as for immunohistological visualization, while, fluorescent anti-rabbit IgG was used as secondary antibody at Ex/Em = 490–500 nm/510–520 nm to provide a green fluorescent tag to the CD-31 positive cells.

2.15. Statistical analysis

Statistical analysis was performed using SigmaPlot 11.0 (San Jose, CA). All statistical data are reported as mean ± standard deviation (S.D.) and comparisons were performed using one-way ANOVA with Tukey's test for multiple comparisons (95% confidence). All groups passed tests for normality and equal variance prior to ANOVA. A p-value of less than 0.05 was considered statistically significant.

3. Results

3.1. In vitro analysis

3.1.1. Culture of hMSC/HUVEC spheroids in vitro

Co-culture hMSC/HUVEC spheroids were loaded within fibrin/PPF composite scaffolds to assess *in vitro* endothelial cell network formation over 1, 2, and 3 weeks of culture. Cellular outgrowth and sprouting were monitored regularly via brightfield microscopy (Fig. 2A–C). At day 0, sprouting is not observed and the spheroid (approximately 250–300 μm diameter) can be seen clearly within the scaffold (Fig. 2A). By day 4, cells begin to reach the edge of the scaffold (Fig. 2B), and by day 7 the cellular outgrowth extends throughout the entire diameter of the scaffold (Fig. 2C). Over the remaining 3 week culture period, cellular outgrowth becomes increasingly dense as cells continue to sprout and proliferate throughout the length of the scaffold.

hMSC/HUVEC network formation was observed in all samples via confocal microscopy and immunofluorescent staining for αSMA and CD31 (Fig. 2D–H) and the area of the CD31-positive network was quantified. Endothelial cell network area increased with culture time (Fig. 2I). Network area at week 3 (1.57 ± 0.27 mm^2) was significantly higher than at week 1 (0.88 ± 0.06 mm^2, $p = 0.007$) and at week 2 (1.03 ± 0.22 mm^2, $p = 0.024$) (Fig. 2I). Vessel-like structures extended to the edge of the scaffold by 3 weeks of culture (Fig. 2F), with hollow lumen-like structures observed after 2 weeks (Fig. 2H). At all timepoints, αSMA staining indicated that hMSCs proliferate through the entire diameter of the scaffold, in addition to significant three-dimensional sprouting. Additionally, hMSCs appeared to closely interact with the HUVEC network (Fig. 2G,H). hMSCs near HUVECs may serve a pericyte-like role, especially after 3 weeks of culture (Fig. 2G).

3.2. In vivo analysis

3.2.1. Human specific CD-31, Masson's trichrome, and H&E staining

The pre-culture groups were implanted in SCID mice after the completion of the respective culture times. After implantation for 9 days, the scaffolds were explanted and histological analysis was performed via immunostaining for human specific CD-31 (an endothelial cell marker), Masson's trichrome staining and H&E staining. As expected, human CD-31 staining was not observed in the control group (Fig. 3i). These images confirm the absence of human endothelial cells within fibrin gels and that the procedure did not result in false positive staining of mouse cells. For samples containing HUVECs, the positive human CD-31 immunostaining is indicated in the higher magnification (Fig. 3(ii–v)) images, respectively. The overall (low magnification) scaffold images of the NP group show that the cells are concentrated at one region indicating the location of the spheroid and vessels containing lumens are hardly visible (Fig. 3(ii)). Vessels with defined lumens can be seen in the remaining groups, i.e., 1P, 2P and 3P. It is also observed that as the pre-culture time increases, the histologically visualized cross-sectional area of the vasculature in the scaffold increases, wherein, 1P group shows concentration of vessels at one particular area (Fig. 3(iii)). The spreading of the vascular network area is seen to increase serially in the 2P and 3P groups.

These human CD-31 stained vascular areas (brown) were further studied with the hematoxylin and eosin (H&E) staining and Masson's trichrome staining via staining of serial sections (Fig. 4). Under H&E staining, the fibrin gel stains pink and the cell nuclei are

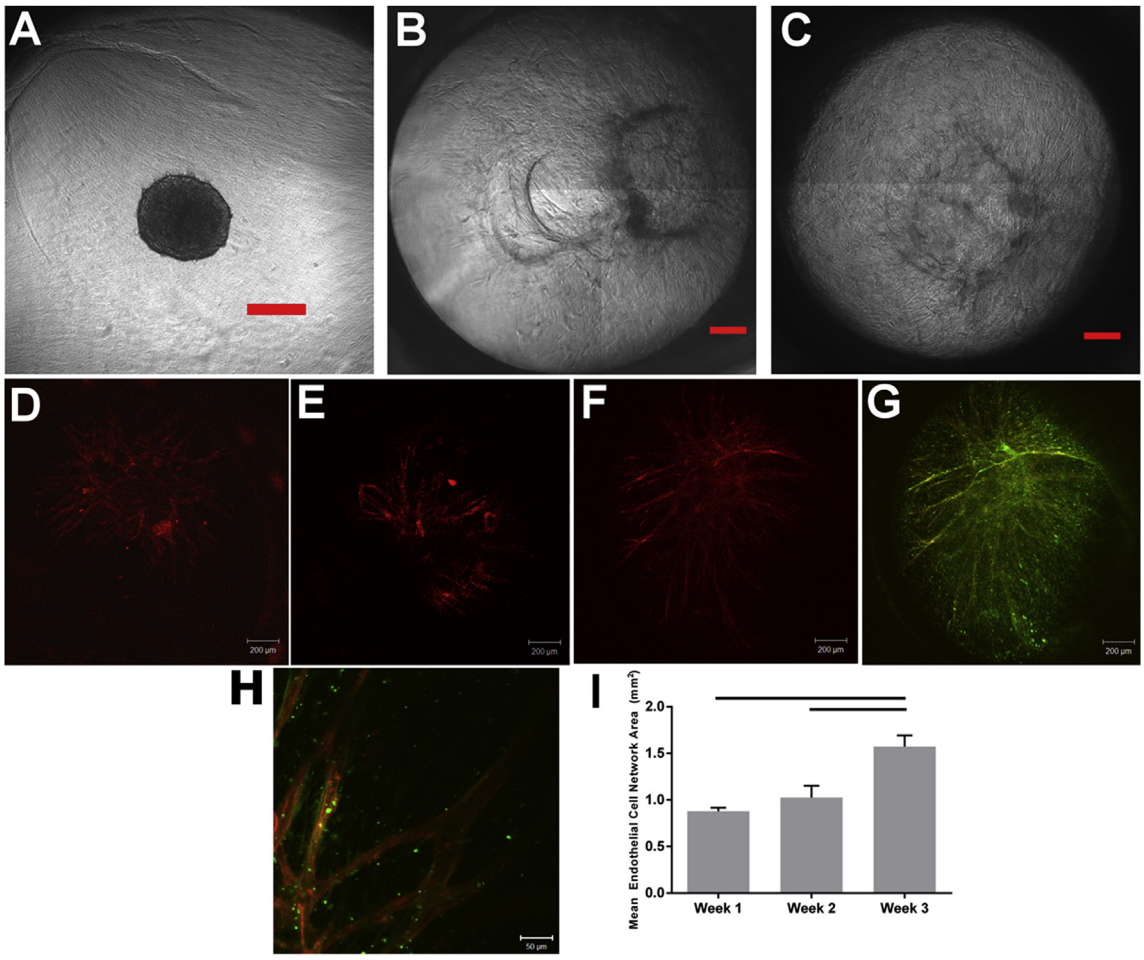

Fig. 2. Intercellular network formation was observed in hMSC/HUVEC spheroids in fibrin/poly(propylene fumarate) composite scaffolds via bright field (A–C) and confocal (D–H) microscopy. Scale bar represents 200 μm in A–G and 50 μm in H. Cells sprout throughout the diameter of the scaffold, as shown in phase contrast images taken at (A) day 0, (B) day 4, and (C) day 7. Immunofluorescent staining was performed for the endothelial cell marker CD31 (TRITC, red) and the hMSC marker α-SMA (FITC, green). Z-stack images were taken using confocal laser-scanning microscopy and two-dimensional projections are shown. CD31-positive vessel-like structures are seen after 1 week (D), 2 weeks (E,H), and 3 weeks (F–G) of culture. (G) CD31/α-SMA merged image shows co-localization of hMSCs with HUVEC sprouts that extend to the edge of the scaffold. (H) CD31/α-SMA merged image shows hMSC/HUVEC interactions and visible lumen-like structures after 2 weeks of culture. (I) CD31-positive stained area was quantified from confocal microscopy images. The area of the endothelial cell network increases with culture time, from 0.88 ± 0.06 mm^2 at week 1, 1.03 ± 0.22 mm^2 at week 2, and 1.57 ± 0.27 mm^2 at week 3. Statistically significant differences were seen between weeks 1 and 3 ($p = 0.007$) and between weeks 2 and 3 ($p = 0.024$), indicated on the graph by a horizontal line. (For interpretation of the references to color in this figure legend, the reader is referred to the web version of this article.)

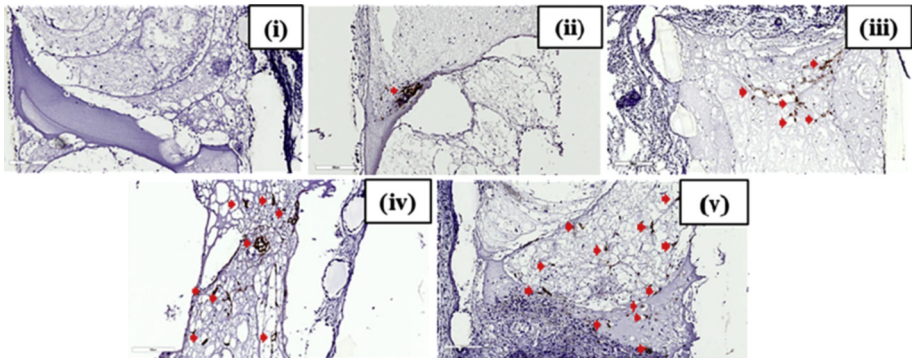

Fig. 3. Human specific CD-31 staining of *in vivo* implanted Poly(propylene fumarate)/Fibrin Scaffolds. The control group (C) did not show any positive staining for endotheial cells depicted by brown staining (i). The no-preculture (ii), 1 week preculture (iii), 2 week pre-culture (iv) and 3 week preculture (v) groups show an increase in vascular area from one group to the next as depicted by brown stained human endothelial cells (indicated by red arrows) mostly forming vessel-like structures in the 1P, 2P and 3P groups as compared to that of NP group, showing positive stained cells accumulated in a single area indicating the presence of spheroids. Scale bar of each image is 300 μm. (For interpretation of the references to color in this figure legend, the reader is referred to the web version of this article.)

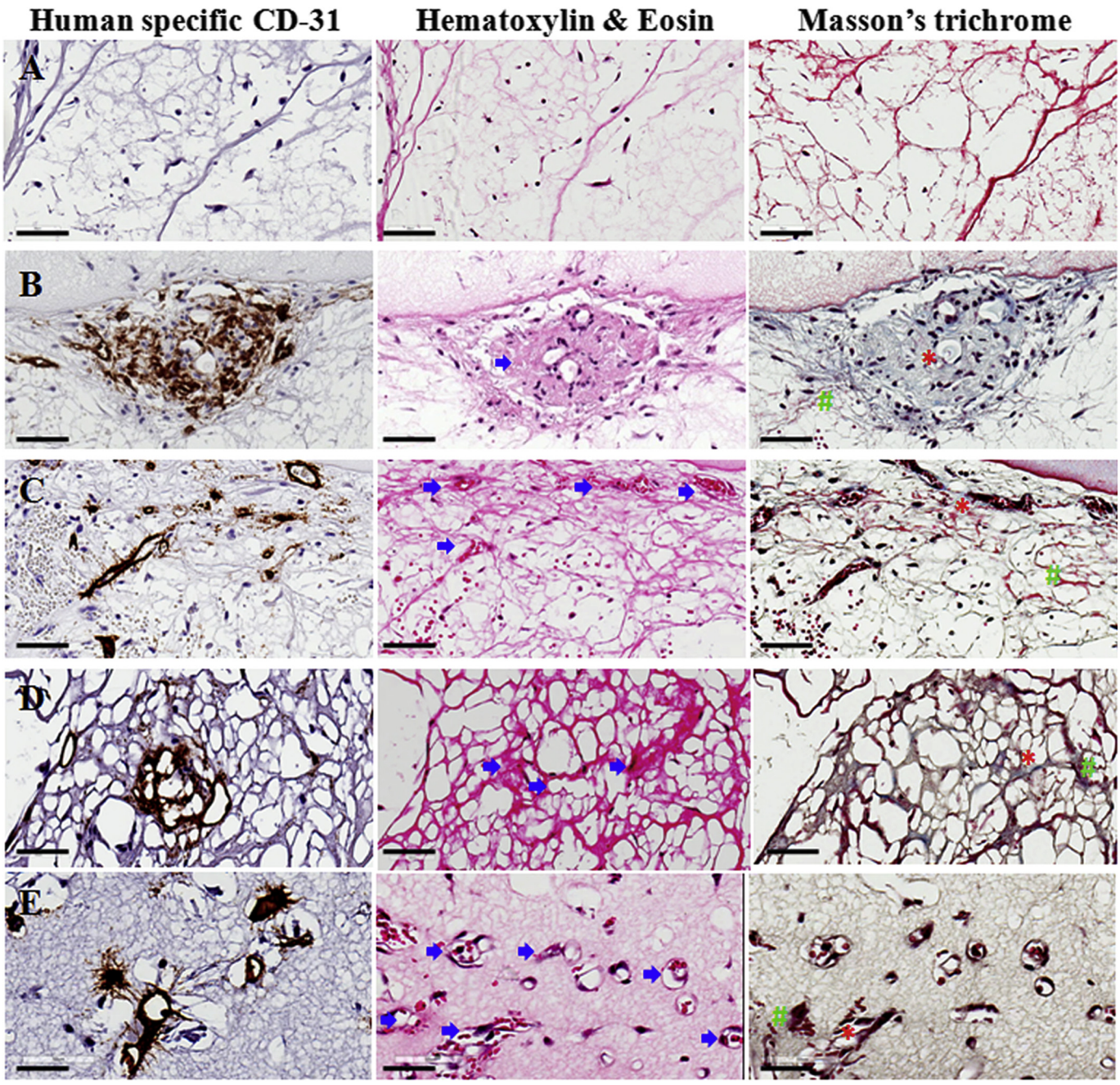

Fig. 4. Image showing the presence of vascular areas via staining of serial sections for human specific CD-31 staining, Hematoxylin & Eosin (H&E) as well as Masson's trichome staining in control (A), no pre-culture (NP) (B), 1 week pre-culture (C), 2 week pre-culture (2P) (D) and 3 week pre-culture (3P) (E) groups. All the groups show large amounts of cells except the control group. The CD-31 immunohistochemistry-stained perfused vascular areas (indicated by blue arrow) can be seen via H&E and Masson's trichrome stain. Masson's trichrome staining also reveals structures such as collagen fibrils (indicated by red '*' symbol) as well as fibrin (indicated by green '#' symbol). The scale bar in each image represents 70 μm. (For interpretation of the references to color in this figure legend, the reader is referred to the web version of this article.)

observed as blue dots. The fibrin in C group (Fig. 4A) shows a typical morphology of fibrin gels with very few nuclei and no signs of vascular areas. Whereas, in the NP (Fig. 4B), 1P (Fig. 4C), 2P (Fig. 4D), and 3P (Fig. 4E) groups, the pink stained thread-like network becomes denser and darker suggesting the presence of collagen fibers. Vascular areas (indicated by blue arrows) are recognized as dark red stained areas associated with blue stained nuclei concentrated at one area in the NP group while these cells are scattered throughout the scaffold in the other groups. In some regions of higher pre-culture groups, these areas show the presence of red blood like cells (red colored dots) filled in the vascular lumen (Fig. 4C–E) indicating the presence of mouse blood which further suggests perfusion of those vessels.

Similarly, in Masson's trichrome staining, vascular areas could be identified as areas containing cells as black colored dots surrounded with bluish-green collagen fibril like structures. Whereas, fibrin is stained red. The indication of the presence of collagenous fibrils is further strengthened by the absence of bluish green fibrils in the C group while bluish green stained regions are found in all other groups, i.e., NP (Fig. 4B), 1P (Fig. 4C), 2P (Fig. 4D), and 3P (Fig. 4E) and fewer red stained fibrils are seen along with the brown stained vascularized areas suggesting the presence of collagen-rich

vascularized tissue. A negligible to mild inflammatory response was observed in all groups.

3.2.2. Quantitative estimation of vessel density

The quantification of vessel density associated with positive human CD-31 immunostaining inside the scaffold through cross-sectional analysis was performed for all five groups (n = 5 for NP, 1P, 3P groups, and, n = 3 for 2P group). We see that the density of positive human CD-31 stained vessels increases from the NP to the 3P group, (Fig. 5). The vessel densities for NP, 1P, 2P and 3P groups are 15.96 ± 5.73, 13.96 ± 7.56, 19.43 ± 16.83 and, 43.68 ± 17.79 vessels per mm^2, respectively. This increase in vessel density is statistically significant between the NP and 3P groups ($p = 0.007$) as well as the 1P and 3P groups ($p = 0.0038$). Hence, the results indicate an increase in the number of human CD-31 positive vessels found *in vivo* with increasing pre-culture time *in vitro*. This further emphasizes the positive effect of *in vitro* pre-culture on *in vivo* vascularization. On the other hand, the control (C) group does not show up in the plot due to 'zero' values obtained for the vessel density signifying the absence of positive human CD-31 stained cells ($p < 0.0001$).

3.2.3. Macroscopic and microscopic lectin imaging

At the macroscopic level, we measured the total fluorescence radiant efficiency of the explanted scaffolds right after the sacrifice of isolectin-injected mice. This allows us to identify vessels that had established blood flow. The extreme groups, i.e., the control and 3P groups were selected for this analysis in order to compare the overall difference from no-spheroid to longest time of spheroid pre-culture. The average total radiant fluorescence efficiency for 3 week pre-culture (3P) and control (C) group is 4.22E + 08 ± 1.12E + 08 and 1.53E + 08 ± 3.49E + 07 photons s^{-1} cm^{-2} $steradian^{-1}$ per μW cm^{-2}, respectively (Fig. 6A). Therefore, the radiant efficiency for the 3 week pre-culture (3P) group scaffolds was significantly higher than the control (C) ($p = 0.0068$). These results are also depicted through representative images from the C and 3P groups (Fig. 6A).

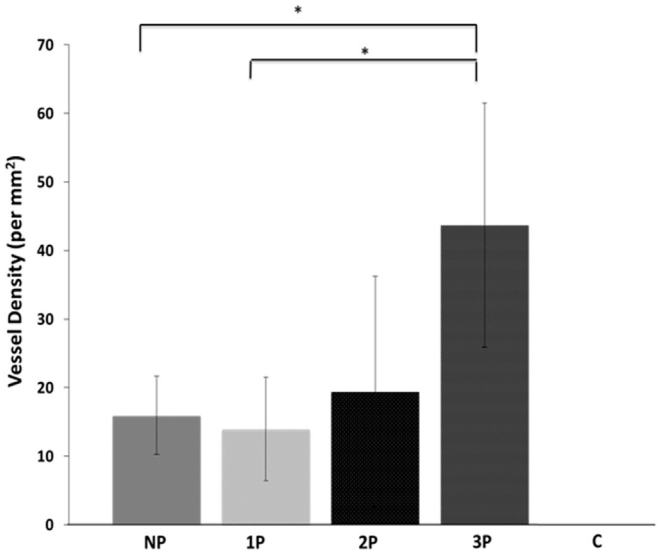

Fig. 5. The plot representing quantification of human CD-31 positive stained vessel density (capillaries/mm^2) in control (C), no pre-culture (NP), 1 week pre-culture (1P), 2 week pre-culture (2P) and 3 week pre-culture (3P) groups. The C group has 'zero' value indicating absence of any human CD-31 positive stained vessels, therefore, its value cannot be seen on the plot. Amongst NP, 1P, 2P and 3P groups, an increasing trend is observed in the vessel density with the increase of pre-culture time. This increase is statistically significant between NP and 3P groups, and, 1P and 3P groups ($^*p < 0.05$).

The fluorescence analysis for positive lectin staining was further performed at a microscopic level for each group (Fig. 6B). For this analysis, we focused on the area inside of the scaffold that contained fibrin along with the spheroid. The control scaffolds did not show any positive staining for lectin (red) fluorescence, while few cells (blue), could be seen in the scaffold that may be the cells penetrating the scaffold from the surrounding host mouse tissue. Therefore, absence of lectin staining inside the C group scaffold but its presence during overall fluorescence analysis of the explanted C group indicates that the mice vessels may be present around the scaffold upon explantation but they have not penetrated enough to provide a positive staining inside the scaffold. In the case of the NP, 1P, 2P and 3P groups, all of the groups show higher cell number as compared to the C group indicating the presence of cells such as hMSCs, HUVECs, or invaded mouse cells. Also, moving from the NP to the 3P group, the positive staining for lectin seems to show an increase along with the spreading of lectin stained regions demonstrating the presence of endothelial cells.

3.2.4. Identification of human endothelial vessels through lectin and human CD-31 co-localization

Image co-localization analysis was performed to evaluate whether lectin perfused vessels inside the scaffold were lined by human endothelial cells. In these images, the lectin is represented by red, human CD-31 by green, and, cell nuclei via blue color fluorescence (Fig. 7), while fibrin is observed through DIC microscopy.

The control group did not show any staining for both lectin and human CD-31 inside the scaffolds, although very few cell nuclei can be seen, those cells may have come from the surrounding host tissue as suggested in the previous section. Also, at the edge of the scaffolds some lectin perfusion was observed due to the integration and penetration of surrounding mouse tissue. The association of lectin and human CD-31 can be clearly seen in the NP, 1P, 2P and 3P groups via yellow color due to co-localization of red lectin and green human CD-31 (Fig. 7). A higher number of cell nuclei are seen than in the control scaffold at and around these vascular areas. Most of these cells are expected to have their origin from HUVECs and hMSCs implanted as spheroids inside the scaffolds. Further, the cell nuclei along with the vascular areas is closely associated with fibrin as it can be seen to ornament fibrin threads.

4. Discussion

The vascularization of scaffolds can be studied in two different contexts, i.e., *in vitro* and *in vivo*. The *in vivo* context can be studied via implantation of a vascular network into the scaffold which then integrates with the surrounding host vascular supply. Another method is performed through implantation at highly vascularized areas of the body such as skin and muscle, leading to vascularization of the scaffold [48]. *In vitro* prevascularization strategies have been shown to be effective in pre-therapeutic research for the establishment a vascular supply and for the subsequent formation, development and integration of bone neo-tissue [28,49–51]. The following two main *in vitro* strategies have been used to vascularize an implant: 1) strategies to recruit/stimulate local vascularization [52,53], 2) *in vitro* prevascularization to form *de novo* blood vessels inside the implant [48]. We use the second strategy in this study to form blood vessels inside the PPF/fibrin solid cured/hydrogel polymeric scaffold system. In comparison to the control (C) group, the explants of all of the other groups (i.e., NP, 1P, 2P and 3P) showed higher levels of vascularization inside the scaffolds (Fig. 3).

Some of the previous studies such as the study by Tsigkou et al. have used the prevascularization strategy for inducing

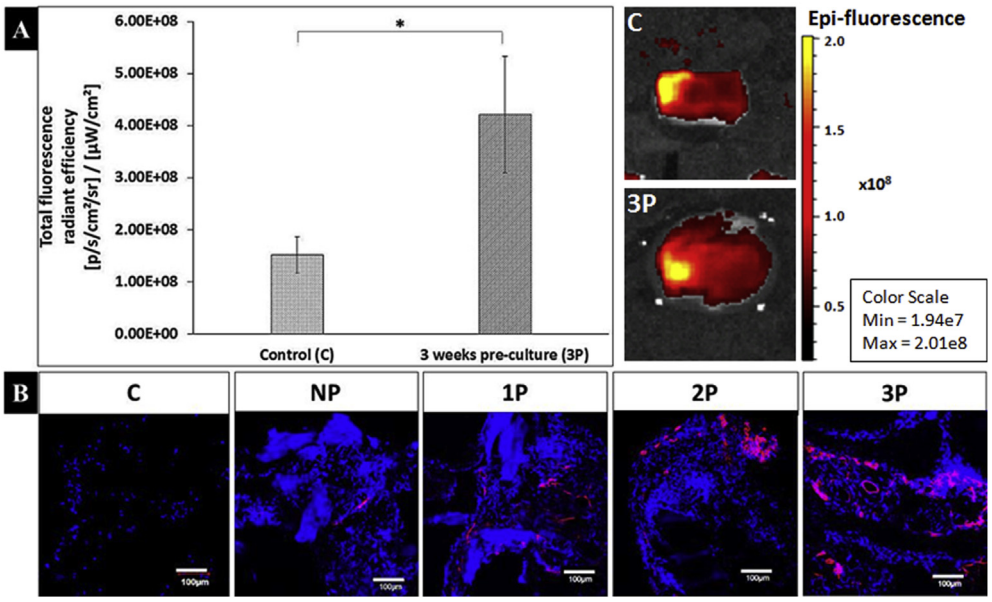

Fig. 6. Macroscopic and microscopic fluorescence analysis for lectin perfusion. (A) Analysis of the explanted scaffolds to quantify the total florescence radiant efficiency after lectin tail vein injection showing significantly (*$p < 0.05$) higher fluorescence value (in photons s^{-1} cm^{-2} $steradian^{-1}$ per µW cm^{-2}) in the 3 week pre-culture (3P) group (4.22E + 08 ± 1.12E + 08) as compared to the control (C) (1.53E + 08 ± 3.49E + 07) group. Representative images of the C and 3P groups are shown to qualitatively demonstrate the difference in fluorescence. (B) Microscopic fluorescence analysis of the positive lectin staining of the vascular areas (red) along with the cell nuclei indicated by dapi staining (blue) at the fibrin area inside the scaffold shows the spreading and increase of vascular networks upon moving sequentially through the no pre-culture (NP), 1 week pre-culture (1P), 2 week pre-culture (2P) and 3 week pre-culture (3P) groups. Here, the control (C) group does not show any positive staining for lectin demonstrating the absence of vessels inside the scaffold. Scale bar for each image is 100 µm. (For interpretation of the references to color in this figure legend, the reader is referred to the web version of this article.)

vascularization along with bone formation but their preculture time was only one day [54]. In this study we found that adding a 'pre-culture' stage, allowing the spheroid cells to organize into networks *in vitro* before implantation for 1–3 weeks improves the quality of subsequent scaffold vascularization (Figs. 3, 5, and 6). Without prevascularization of the scaffold, it may take too long to form the vasculature upon implantation which would result in an ischemic condition before the desired neo-bone could form and integrate into the defect site [55]. Absence of a uniform vasculature is especially detrimental for scaffolds of clinically relevant sizes. It is expected that our strategy would promote uniform vascularization of large defects (i.e., clinically relevant sizes). Though, in order to scale-up our study to the level of clinically relevant sizes we may face challenges in our current study design. One of these can be the requirement to increase the prevascularization period in order to accommodate the increase in size which in turn may affect cell survivability. We plan to address this problem by incorporation of more than one spheroid leading to an increase in the number of sprouting points in the overall system.

Spheroids of HUVECs and hMSCs make a stable vascular system due to the formation of vessels under the support of MSCs [56]. During our *in vitro* studies, we observed extensive intercellular network formation of hMSCs and HUVECs. hMSCs were observed to migrate and sprout throughout a large portion of the scaffold after three weeks of culture. Within this hMSC network, extensive vascular-like structures were formed by the HUVECs, with three-dimensional vessel sprouting that extended to the edge of the scaffold in a three-week culture period. Following implantation, these vessels were shown to be stable and capable of anastomosing with the host vasculature as indicated by lectin-perfused human-CD31-positive staining. Therefore, our study provides a method to increase early vascular formation and perfusion upon *in vivo* implantation of HUVEC/hMSC spheroids in a PPF/fibrin composite scaffold system.

For bone tissue engineering, both vascularization and bone formation are important for the success of tissue engineered bone grafts. For vascularization, stiffer gels are less preferred over soft gels, which allow higher vessel formation [57]. However, traditionally, stiffer materials have been preferred for bone progenitor cell differentiation to the bone lineage [58]. Therefore, our composite scaffold system is favorable in the sense that it provides a softer hydrogel medium of fibrin that is favorable for vascular sprouting, and, a stiffer matrix made of PPF to support maintenance of the bone defect site and initial bone ingrowth. However, we would also like to ensure that the solid cured component is able to resorb in time to allow remodeling of the neo-bone as that is the only way that strong, long-lasting bone will form. Finally we expect that the PPF/fibrin composite system could be a good strategy for vascularized bone formation.

Our results demonstrate that vasculature infusion inside the scaffold does not occur with a fibrin-loaded solid-cured PPF shell alone. The presence of a hMSC/HUVEC spheroid assists vascular infusion that increases as spheroid pre-culture time increases from no-pre-culture to 3 weeks of pre-culture.

5. Conclusions

This study evaluates the potential of a PPF/fibrin composite scaffold system for the prevascularization of bone tissue engineering scaffolds. It assesses the possibility of *in vitro* pre-culture to ensure early and uniform vascularization following *in vivo* implantation. In the future, we intend to study the effect of pre-vascularization on bone formation. It will also be important to determine whether parameters such as the size and number of spheroids, and their location in the matrix and the geometry of the PPF scaffold, can be optimized to ensure maximum output in terms of vascularization and subsequent bone formation and remodeling. Once optimized, these parameters will help in evaluating the time required for complete vascularization of tissue engineered grafts employed for the healing of critical size and larger bone defects.

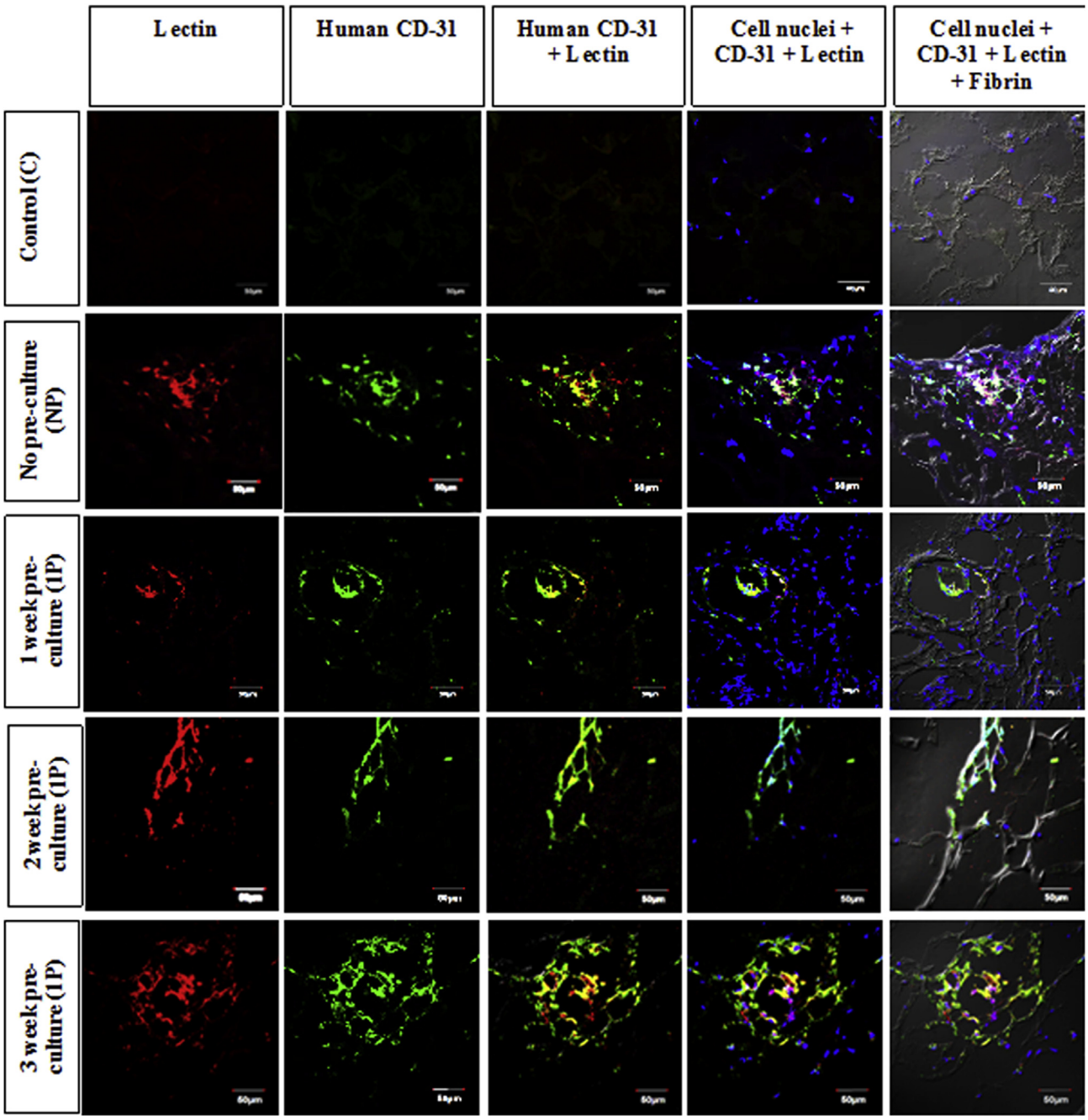

Fig. 7. Lectin and human CD-31 double staining for the analysis of perfused vessels that are made of human endothelial cells. The control (C), no pre-culture (NP), 1 week pre-culture (1P), 2 week pre-culture (2P) and 3 week pre-culture (3P) groups are observed for lectin and human CD-31 staining. The image shows that both types of stain co-localize in all the groups except the controls suggesting the presence of perfused human endothelial vessels in the pre-culture groups, i.e., NP, 1P, 2P and 3P. Also, presence of fibrin (via differential interference contrast microscopy) and cell nuclei (via DAPI staining) is also depicted at the same area which further indicates the association of cells and fibrin with the lectin and CD-31 stained cells. Scale bar for each image is 50 μm.

Disclosure statement

No Conflicts of Interest to disclose.

Acknowledgments

This work was partially supported by NIH Grant R01-AR061460 and the Veterans Administration. We would like to thank Prof. Matthew Becker (Department of Polymer Science, University of Akron, Akron, OH) for providing the PPF resin used in this study. We also acknowledge the support that the James Comprehensive Cancer Center (Ohio State University, Columbus, USA) received from NIH grant P30 CA016058 along with the efforts of Ms. Florinda Jaynes at the Comparative Pathology and Mouse Phenotyping facility. Confocal microscopy and image analysis were performed at the Campus Microscopy Imaging Facility (Ohio State University, Columbus, USA). We wish to thank the Small Animal Imaging Core (SAIC) (Ohio State University, Columbus, USA) for access to the *in vivo* imaging system (IVIS Lumina II) and analysis for lectin fluorescence. The authors would also like to thank Ms. Brianna Swan for helping with animal surgeries and husbandry, Ms. Jacqueline Stewart for helping with tail vein injections, and Mr. Eric

Mott and Ms. Courtney Dolder for helping with 3-D printing of the scaffolds.

References

[1] D.J. Hadjidakis, I.I. Androulakis, Bone remodeling, Ann. N. Y. Acad. Sci. 1092 (2006) 385–396.
[2] F. Barrere, C.A. van Blitterswijk, K. de Groot, Bone regeneration: molecular and cellular interactions with calcium phosphate ceramics, Int. J. Nanomedicine 1 (2006) 317–332.
[3] S. Bose, M. Roy, A. Bandyopadhyay, Recent advances in bone tissue engineering scaffolds, Trends Biotechnol. 30 (2012) 546–554.
[4] A.R. Amini, C.T. Laurencin, S.P. Nukavarapu, Bone tissue engineering: recent advances and challenges, Crit. Rev. Biomed. Eng. 40 (2012) 363–408.
[5] L. Krishnan, N.J. Willett, R.E. Guldberg, Vascularization strategies for bone regeneration, Ann. Biomed. Eng. 42 (2014) 432–444.
[6] Y. Liu, J. Lim, S.H. Teoh, Review: development of clinically relevant scaffolds for vascularised bone tissue engineering, Biotechnol. Adv. 31 (2013) 688–705.
[7] E.C. Novosel, C. Kleinhans, P.J. Kluger, Vascularization is the key challenge in tissue engineering, Adv. Drug Deliv. Rev. 63 (2011) 300–311.
[8] Y. Liu, J.K. Chan, S.H. Teoh, Review of vascularised bone tissue-engineering strategies with a focus on co-culture systems, J. Tissue Eng. Regen. Med. 9 (2015) 85–105.
[9] Y. Naito, T. Shinoka, D. Duncan, N. Hibino, D. Solomon, M. Cleary, et al., Vascular tissue engineering: towards the next generation vascular grafts, Adv. Drug Deliv. Rev. 63 (2011) 312–323.
[10] K.Y. Lee, M.C. Peters, K.W. Anderson, D.J. Mooney, Controlled growth factor release from synthetic extracellular matrices, Nature 408 (2000) 998–1000.
[11] M. Lovett, K. Lee, A. Edwards, D.L. Kaplan, Vascularization strategies for tissue engineering, Tissue Eng. Part B Rev. 15 (2009) 353–370.
[12] L.S. Gardel, L.A. Serra, R.L. Reis, M.E. Gomes, Use of perfusion bioreactors and large animal models for long bone tissue engineering, Tissue Eng. Part B Rev. 20 (2014) 126–146.
[13] W.L. Grayson, M. Frohlich, K. Yeager, S. Bhumiratana, M.E. Chan, C. Cannizzaro, et al., Engineering anatomically shaped human bone grafts, Proc. Natl. Acad. Sci. U. S. A. 107 (2010) 3299–3304.
[14] W.L. Grayson, S. Bhumiratana, C. Cannizzaro, G. Vunjak-Novakovic, Bioreactor cultivation of functional bone grafts, Methods Mol. Biol. 698 (2011) 231–241.
[15] J. Kim, T. Ma, Bioreactor strategy in bone tissue engineering: pre-culture and osteogenic differentiation under two flow configurations, Tissue Eng. Part A 18 (2012) 2354–2364.
[16] J. Rauh, F. Milan, K.P. Gunther, M. Stiehler, Bioreactor systems for bone tissue engineering, Tissue Eng. Part B Rev. 17 (2011) 263–280.
[17] A.B. Yeatts, J.P. Fisher, Bone tissue engineering bioreactors: dynamic culture and the influence of shear stress, Bone 48 (2011) 171–181.
[18] R.R. Rao, J.P. Stegemann, Cell-based approaches to the engineering of vascularized bone tissue, Cytotherapy 15 (2013) 1309–1322.
[19] Y. Liu, S.H. Teoh, M.S. Chong, C.H. Yeow, R.D. Kamm, M. Choolani, et al., Contrasting effects of vasculogenic induction upon biaxial bioreactor stimulation of mesenchymal stem cells and endothelial progenitor cells cocultures in three-dimensional scaffolds under in vitro and in vivo paradigms for vascularized bone tissue engineering, Tissue Eng. Part A 19 (2013) 893–904.
[20] R.E. Unger, S. Ghanaati, C. Orth, A. Sartoris, M. Barbeck, S. Halstenberg, et al., The rapid anastomosis between prevascularized networks on silk fibroin scaffolds generated in vitro with cocultures of human microvascular endothelial and osteoblast cells and the host vasculature, Biomaterials 31 (2010) 6959–6967.
[21] R.E. Unger, E. Dohle, C.J. Kirkpatrick, Improving vascularization of engineered bone through the generation of pro-angiogenic effects in co-culture systems, Adv. Drug Deliv. Rev. (2015), http://dx.doi.org/10.1016/j.addr.2015.03.012 (eProof), http://www.ncbi.nlm.nih.gov/pubmed/25817732.
[22] A. Wenger, A. Stahl, H. Weber, G. Finkenzeller, H.G. Augustin, G.B. Stark, et al., Modulation of in vitro angiogenesis in a three-dimensional spheroidal coculture model for bone tissue engineering, Tissue Eng. 10 (2004) 1536–1547.
[23] S.H. Hsu, T.T. Ho, N.C. Huang, C.L. Yao, L.H. Peng, N.T. Dai, Substrate-dependent modulation of 3D spheroid morphology self-assembled in mesenchymal stem cell-endothelial progenitor cell coculture, Biomaterials 35 (2014) 7295–7307.
[24] C. Correia, W.L. Grayson, M. Park, D. Hutton, B. Zhou, X.E. Guo, et al., In vitro model of vascularized bone: synergizing vascular development and osteogenesis, PLoS One 6 (2011) e28352.
[25] C.J. Kirkpatrick, S. Fuchs, R.E. Unger, Co-culture systems for vascularization—learning from nature, Adv. Drug Deliv. Rev. 63 (2011) 291–299.
[26] E. Fennema, N. Rivron, J. Rouwkema, C. van Blitterswijk, J. de Boer, Spheroid culture as a tool for creating 3D complex tissues, Trends Biotechnol. 31 (2013) 108–115.
[27] F.A. Saleh, M. Whyte, P.G. Genever, Effects of endothelial cells on human mesenchymal stem cell activity in a three-dimensional in vitro model, Eur. Cell Mater 22 (2011) 242–257.
[28] J. Rouwkema, J. de Boer, C.A. Van Blitterswijk, Endothelial cells assemble into a 3-dimensional prevascular network in a bone tissue engineering construct, Tissue Eng. 12 (2006) 2685–2693.
[29] S.J. Bidarra, C.C. Barrias, M.A. Barbosa, R. Soares, J. Amedee, P.L. Granja, Phenotypic and proliferative modulation of human mesenchymal stem cells via crosstalk with endothelial cells, Stem Cell Res. 7 (2011) 186–197.
[30] M.E. Francis-Sedlak, M.L. Moya, J.J. Huang, S.A. Lucas, N. Chandrasekharan, J.C. Larson, M.H. Cheng, E.M. Brey, Collagen glycation alters neovascularization in vitro and in vivo, Microvasc. Res. 80 (2010) 3–9.
[31] B.M. Roux, M.H. Cheng, E.M. Brey, Engineering clinically relevant volumes of vascularized bone, J. Cell Mol. Med. 19 (2015) 903–914.
[32] L.F. Mendes, R.P. Pirraco, W. Szymczyk, A.M. Frias, T.C. Santos, R.L. Reis, et al., Perivascular-like cells contribute to the stability of the vascular network of osteogenic tissue formed from cell sheet-based constructs, PLoS One 7 (2012) e41051.
[33] D. Dean, J. Wallace, A. Siblani, M.O. Wang, K. Kim, A.G. Mikos, et al., Continuous Digital Light Processing (cDLP): highly accurate additive manufacturing of tissue engineered bone scaffolds, Virtual Phys. Prototyp. 7 (2012) 13–24.
[34] M.O. Wang, C.E. Vorwald, M.L. Dreher, E.J. Mott, M.H. Cheng, A. Cinar, et al., Evaluating 3D-printed biomaterials as scaffolds for vascularized bone tissue engineering, Adv. Mater 27 (2015) 138–144.
[35] K. Kim, D. Dean, J. Wallace, R. Breithaupt, A.G. Mikos, J.P. Fisher, The influence of stereolithographic scaffold architecture and composition on osteogenic signal expression with rat bone marrow stromal cells, Biomaterials 32 (2011) 3750–3763.
[36] J.W. Vehof, J.P. Fisher, D. Dean, J.P. van der Waerden, P.H. Spauwen, A.G. Mikos, et al., Bone formation in transforming growth factor beta-1-coated porous poly(propylene fumarate) scaffolds, J. Biomed. Mater Res. 60 (2002) 241–251.
[37] J.P. Fisher, M.D. Timmer, T.A. Holland, D. Dean, P.S. Engel, A.G. Mikos, Photoinitiated cross-linking of the biodegradable polyester poly(propylene fumarate). Part I. Determination of network structure, Biomacromolecules 4 (2003) 1327–1334.
[38] D. Dean, M.S. Wolfe, Y. Ahmad, A. Totonchi, J.E. Chen, J.P. Fisher, et al., Effect of transforming growth factor beta 2 on marrow-infused foam poly(propylene fumarate) tissue-engineered constructs for the repair of critical-size cranial defects in rabbits, Tissue Eng. 11 (2005) 923–939.
[39] Z.S. Patel, S. Young, Y. Tabata, J.A. Jansen, M.E. Wong, A.G. Mikos, Dual delivery of an angiogenic and an osteogenic growth factor for bone regeneration in a critical size defect model, Bone 43 (2008) 931–940.
[40] A.J. Melchiorri, N. Hibino, J.P. Fisher, Strategies and techniques to enhance the in situ endothelialization of small-diameter biodegradable polymeric vascular grafts, Tissue Eng. Part B Rev. 19 (2013) 292–307.
[41] A.J. Melchiorri, N. Hibino, Z.R. Brandes, R.A. Jonas, J.P. Fisher, Development and assessment of a biodegradable solvent cast polyester fabric small-diameter vascular graft, J. Biomed. Mater Res. A 102 (2014) 1972–1981.
[42] A.J. Melchiorri, N. Hibino, T. Yi, Y.U. Lee, T. Sugiura, S. Tara, et al., Contrasting biofunctionalization strategies for the enhanced endothelialization of biodegradable vascular grafts, Biomacromolecules 16 (2015) 437–446.
[43] L.G. Bracaglia, L. Yu, N. Hibino, J.P. Fisher, Reinforced pericardium as a hybrid material for cardiovascular applications, Tissue Eng. Part A 20 (2014) 2807–2816.
[44] B. Jiang, T.M. Waller, J.C. Larson, A.A. Appel, E.M. Brey, Fibrin-loaded porous poly(ethylene glycol) hydrogels as scaffold materials for vascularized tissue formation, Tissue Eng. Part A 19 (2013) 224–234.
[45] M.A. Shuman, D.M. Tollefsen, P.W. Majerus, The binding of human and bovine thrombin to human platelets, Blood 47 (1976) 43–54.
[46] T.C. Lee, T.H. Lee, Y.H. Huang, N.K. Chang, Y.J. Lin, P.W.C. Chien, et al., Comparison of surface markers between human and rabbit mesenchymal stem cells, PLoS One 9 (2014) e111390.
[47] B. Gottenbos, F. Klatter, H.C. Van Der Mei, H.J. Busscher, P. Nieuwenhuis, Late hematogenous infection of subcutaneous implants in rats, Clin. Diagn. Lab. Immunol. 8 (2001) 980–983.
[48] N.C. Rivron, J.J. Liu, J. Rouwkema, J. de Boer, C.A. van Blitterswijk, Engineering vascularised tissues in vitro, Eur. Cell Mater. 15 (2008) 27–40.
[49] W.L. Dissanayaka, L. Zhu, K.M. Hargreaves, L. Jin, C. Zhang, In vitro analysis of scaffold-free prevascularized microtissue spheroids containing human dental pulp cells and endothelial cells, J. Endod. 41 (2015) 663–670.
[50] X. Chen, A.S. Aledia, C.M. Ghajar, C.K. Griffith, A.J. Putnam, C.C. Hughes, et al., Prevascularization of a fibrin-based tissue construct accelerates the formation of functional anastomosis with host vasculature, Tissue Eng. Part A 15 (2009) 1363–1371.
[51] P. Au, J. Tam, D. Fukumura, R.K. Jain, Bone marrow-derived mesenchymal stem cells facilitate engineering of long-lasting functional vasculature, Blood 111 (2008) 4551–4558.
[52] O. Tsigkou, I. Pomerantseva, J.A. Spencer, P.A. Redondo, A.R. Hart, E. O'Doherty, et al., Engineered vascularized bone grafts, Proc. Natl. Acad. Sci. U. S. A. 107 (2010) 3311–3316.
[53] B. Akar, B. Jiang, S.I. Somo, A.A. Appel, J.C. Larson, K.M. Tichauer, E.M. Brey, Biomaterials with persistent growth factor gradients in vivo accelerate vascularized tissue formation, Biomaterials 72 (2015) 61–73.
[54] S.I. Somo, B. Akar, E.S. Bayrak, J.C. Larson, A.A. Appel, H. Mehdizadeh, et al., Pore interconnectivity influences growth factor-mediated vascularization in sphere-templated hydrogels, Tissue Eng. Part C 21 (2015) 773–785.
[55] A.E. Mercado-Pagan, A.M. Stahl, Y. Shanjani, Y. Yang, Vascularization in bone

tissue engineering constructs, Ann. Biomed. Eng. 43 (2015) 718–729.
[56] K. Rahul, M.V. Singh, Andrew J. Putnam, Mesenchymal support cells in the assembly of functional vessel networks, in: E.M. Brey (Ed.), Vascularization, CRC Press, Taylor & Francis Group, Boca Raton, FL, 2015.
[57] A.L. Sieminski, R.P. Hebbel, K.J. Gooch, The relative magnitudes of endothelial force generation and matrix stiffness modulate capillary morphogenesis in vitro, Exp. Cell Res. 297 (2004) 574–584.
[58] A.J. Engler, S. Sen, H.L. Sweeney, D.E. Discher, Matrix elasticity directs stem cell lineage specification, Cell 126 (2006) 677–689.